Analysis of charged acrylic particles by on-line comprehensive two-dimensional liquid chromatography and automated data-processing

Pirok, B.W.J.; Abdulhussain, N.; Brooijmans, T.; Nabuurs, T.; de Bont, J.; Schellekens, M.A.J.; Peters, R.A.H.; Schoenmakers, P.J.

DOI
10.1016/j.aca.2018.12.059

Publication date
2019

Document Version
Final published version

Published in
Analytica Chimica Acta

Analytica Chimica Acta 1054 (2019) 184–192

Contents lists available at ScienceDirect

Analytica Chimica Acta

journal homepage: www.elsevier.com/locate/aca

Analysis of charged acrylic particles by on-line comprehensive two-dimensional liquid chromatography and automated data-processing

Bob W.J. Pirok [a, b, *], Noor Abdulhussain [a], Ton Brooijmans [c], Tijs Nabuurs [c], Jens de Bont [c], Mike A.J. Schellekens [c], Ron A.H. Peters [a, c], Peter J. Schoenmakers [a]

[a] University of Amsterdam, van 't Hoff Institute for Molecular Sciences, Analytical-Chemistry Group, Science Park 904, 1098 XH, Amsterdam, the Netherlands
[b] TI-COAST, Science Park 904, 1098 XH, Amsterdam, the Netherlands
[c] DSM Coating Resins, Sluisweg 12, 5145 PE, Waalwijk, the Netherlands

HIGHLIGHTS

- Comprehensive 2D-LC was used to characterize polymeric nanoparticles.
- The relation between particle size and composition was determined.
- Applicable to hydrophobic, hydrophilic and charged monomer-comprising particles.
- An algorithm was developed to automatically correct for HDC band broadening.
- Method can be used to study particle formation during emulsion polymerization.

GRAPHICAL ABSTRACT

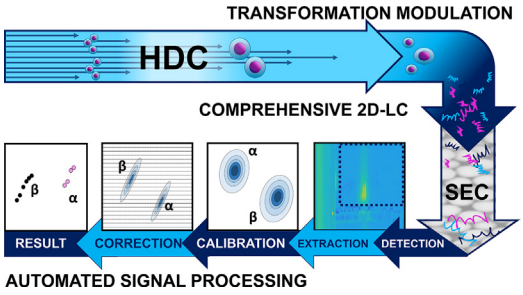

ARTICLE INFO

Article history:
Received 3 November 2018
Received in revised form
21 December 2018
Accepted 26 December 2018
Available online 9 January 2019

Keywords:
On-line dissolution
LC×LC
Hydrodynamic chromatography
Stationary-phase-assisted modulation
Band-broadening correction
Curve-resolution signal processing

ABSTRACT

A thorough understanding of particle formation and polymer growth during emulsion polymerization is indispensable for the development of particles and products with very specific properties. This has created a demand for the detailed characterization of various properties and property distributions – and the relation between these. A method is described that enables comprehensive, simultaneous determination of the size distribution of nanoparticles and the molecular-weight distribution of the constituting polymers as a function of the particle size. The result is a complete two-dimensional distribution that details the interdependence of the two parameters. The approach comprehensively combines hydrodynamic chromatography with size-exclusion chromatography. An automated band-broadening filter has been developed to improve the accuracy of the measured distributions. The algorithm utilizes automated curve-fitting approaches to describe detected particle distributions for each horizontal slice of the 2D-LC chromatogram, and filters band broadening using calibration curves. The method has been applied to samples of complex nanoparticles comprising hydrophobic, hydrophilic and charged moieties, *viz.* stabilized dispersions of poly[(methyl methacrylate)-*co*-(butyl acrylate)-*co*-(methacrylic acid)]-nanoparticles in water. We consistently found that, within a single population of particles, the weight-average molecular weight increases with particle size.

* Corresponding author. Science Park 904, 1098 XH, Amsterdam, the Netherlands.
E-mail address: B.W.J.Pirok@uva.nl (B.W.J. Pirok).

https://doi.org/10.1016/j.aca.2018.12.059
0003-2670/

1. Introduction

Polymeric nanoparticle dispersions are widely applied in a variety of applications including in drug delivery [1,2], coatings [3] and electronics [4]. Depending on the starting composition and applied preparation technique, nanoparticles can be equipped with various colloidal and physicochemical properties [5]. In 1974, Hamish Small used hydrodynamic chromatography (HDC) to investigate and measure particle growth kinetics in emulsion polymerization. HDC is still a popular technique used for the assessment of particle-size distributions [6]. While a large range of other analytical techniques exist for the determination of various properties, simultaneous determination of multiple properties and the relation between these is still challenging. One analytical technique potentially capable of determining multiple properties, or sample dimensions [7], is comprehensive two-dimensional liquid chromatography (LC×LC) [8].

In typical LC×LC, two orthogonal (*i.e.* vastly different) separations are coupled through a modulation interface [9]. The modulator is often a two-position 8-port or 10-port switching valve, equipped with two storage loops which alternatingly take fractions of the first-dimension (^{1}D) effluent and inject these into a second-dimension (^{2}D) separation. The period between valve switches is commonly referred to as the modulation time (t_{mod}). For comprehensive 2D-LC the premise is that all first-dimension effluent is subjected to a second-dimension separation. This premise requires the ^{2}D separation to be completed before injection of the next ^{1}D fraction. Also, in truly comprehensive 2D-LC (LC×LC) none of the separation that has been achieved in the first dimension is lost. This poses requirements on the number of fractions that must be collected (ideally, 2 to 3 per first-dimension peak [10,11]). The modulation time thus depends on the first-dimension peak capacity and analysis time. The required loop volume also depends strongly on the ^{1}D flow rate. The loop must allow storage of the full volume of ^{1}D effluent during one modulation time [12].

Our previous work combined HDC with size-exclusion chromatography (SEC) to simultaneously determine the particle-size distribution (PSD) and the molecular-weight distribution (MWD) of the constituting polymers. To ensure compatibility of the aqueous ^{1}D HDC with the organic ^{2}D SEC and to ensure effective dissolution of the particles, we utilized stationary-phase-assisted modulation (SPAM) with C18 trap cartridges in the modulator loops. We established a framework for particle-analysis methods using LC×LC, by studying nanoparticles comprising relatively simple and relatively hydrophobic polystyrene (PS) and poly(-methyl methacrylate) (PMMA) polymers. Typical nanoparticle applications, however, feature colloidal dispersions of complex (statistical) copolymers which comprise two or more different monomers. These copolymers may feature hydrophilic or even charged monomer units, which would jeopardize the characterization according to our previous SPAM method, because polymers containing charged, hydrophilic units are very difficult to trap.

Another problem concerns data processing of the obtained 2D chromatograms. The analysis of standards with a certified narrow PSD resulted in rather broad HDC peaks and therefore, seemingly broad PSDs. This dramatic band broadening is a known problem in HDC, for which band-broadening-correction algorithms have been developed [13]. While such algorithms may feasibly also be applied to LC×LC data, it is important to consider that an LC×LC chromatogram comprises a number (n) of stacked virtual HDC chromatograms (or "slices") that is equal to

$$n = f_{det} \cdot t_{mod} \quad (1)$$

Here, f_{det} is the sampling rate of the detector. For a typical HDC×SEC separation, with a modulation time of 30 s and an acquisition rate of 160 Hz, one analysis will thus generate 4800 virtual HDC chromatograms. For each of these slices, the HDC time axis must be translated to a particle-size axis through calibration, after which band-broadening correction must be carried out. The applied algorithms must correctly detect the presence and shape of all (co-eluting) distributions and reduce their band widths independently using the correct function.

In this work, we developed an LC×LC-based separation system which is universally applicable to polymeric particles comprising hydrophobic, hydrophilic and/or carboxylic acid functional polymers. We will clarify the necessary adjustments made to our previously published platform, demonstrate an automated data-processing algorithm, and apply the resulting method to a number of industrial nanoparticle formulations.

2. Experimental

2.1. Instrumental

2.1.1. Equipment

All experiments were carried out on an Agilent 1290 Infinity 2D-LC system (Agilent Waldbronn, Germany). For solvent delivery, the system comprised two binary pumps (G4220A, Pumps A and D), one 1200 series isocratic pump (G1310A, Pump B) and an 1100 series isocratic pump (G1310A, Pump C). Other system components included an autosampler (G4226A), two thermostatted column compartments (G1316C), each equipped with a 2D-LC 8-port, 2-position modulation valve (G4236A), an 1260 evaporative light-scattering detector (ELSD, G4260B) and two diode-array detectors (DAD, G4212A). The DADs were equipped with Agilent Max-Light Cartridge Cells (G4212-60008, 10-mm path length, $V_{det} = 1.0$ μL). The injector needle drew and ejected at a speed of 10 μL min^{-1} with two seconds equilibration time. All tubing was fabricated of stainless steel. The chromatographic system was controlled using Agilent OpenLAB CDS Chemstation Edition (Rev. C.01.04) software.

The first-dimension column was an Agilent PL-PSDA cartridge type-1 (800 × 7.5 mm i.d.) for the HDC separation. The second-dimension column was an Agilent PLGel MIXED-C (150 × 4.6 mm i.d., $d_p = 5$ μm) column for the SEC separation. For trapping, Phenomenex SecurityGuard ULTRA (P/N: AJ0-9000) guard-column holders were used in conjunction with UHPLC C18 2.1-mm i.d. SecurityGuard ULTRA cartridges (P/N: AJ0-8782). Each trap was directly installed into one of the ports of the valve with the male end, the female end was connected to another port using a 140-mm long SS tubing with 0.12 mm i.d.

2.1.2. Configuration of the chromatographic system

In the LC×LC experiments, the HDC effluent was transported to one of the 8-port valves using a fused-silica capillary (see Fig. 1). This narrow (75 μm i.d.) 300-mm long capillary was used to generate sufficient restriction to prevent THF from migrating into the polymer-particle-packed HDC column and damaging the packing. The valve allowed the first approximately 11.9 mL of HDC effluent to be diverted to the waste, leaving approximately 1.8 mL of analyte-containing effluent to process by the LC×LC system. After passing through the first 8-port valve, effluent from the HDC column was continuously combined with a flow of THF. The combined flow was mixed in Mixer 1 (Agilent Jet Weaver V100 mixer, P/N: G4220-60006, internal volume 100 μL). The mixed HDC-buffer/THF stream was in turn combined with an acidic 10 mM ammonium formate/formic acid buffer (pH = 3.0) in Mixer 2 (Waters Zirconia 50 μL Y-mixer, P/N: 700002911, internal volume 50 μL). The resulting flow was then routed to the second 8-port valve containing the traps.

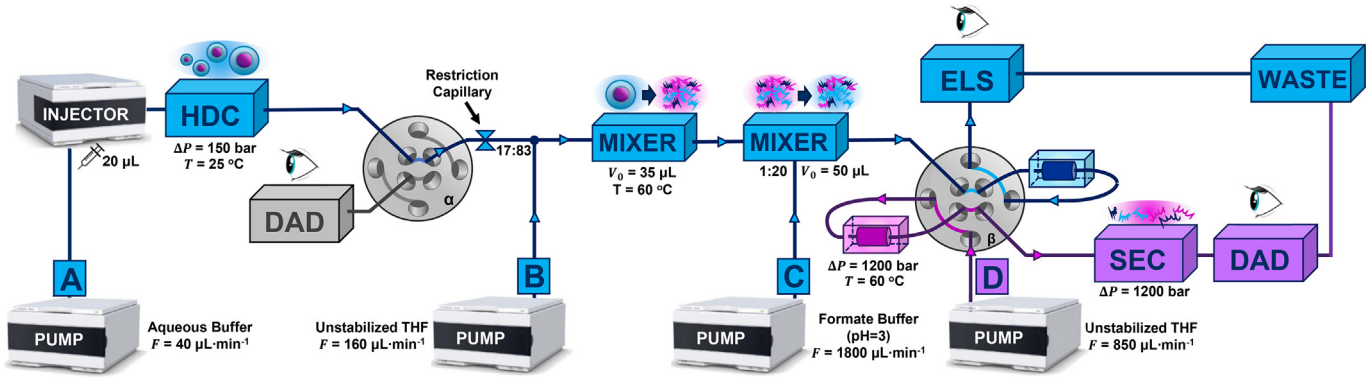

Fig. 1. Scheme detailing the utilized chromatographic setup for nanoparticle analysis. For explanation see text.

2.2. Chemicals

Non-stabilized tetrahydrofuran (THF, HPLC-S grade) was obtained from Biosolve (Valkenswaard, The Netherlands). Sodium dihydrogen phosphate (Cat. no.: 106346, monohydrate) was obtained from Merck (Darmstadt, Germany). Sodium dodecyl sulphate (SDS, Cat. no.: L4509-250G), Trifluoroacetic acid (TFA), Brij 35 non-ionic surfactant (Cat. no.: B4184-1L, described as a 30% w/v solution) and sodium azide (Cat. no.: S2002-100G) were obtained from Sigma-Aldrich (Darmstadt, Germany). Polystyrene standards (PS) for determining calibration curves were obtained from Polymer Laboratories (now Agilent Technologies, Church Stretton, Shropshire, UK). The 3000 series Nanosphere polystyrene nanoparticle standards were obtained from ThermoFisher Scientific (Bremen, Germany). The particle diameters were: 350 ± 6 nm (P/N: 3500A), 216 ± 4 nm (P/N: 3220A), 203 ± 5 nm (P/N:3200A), 100 ± 3 nm (P/N: 3100A), 46 ± 2 nm (P/N: 3050A) and 30 ± 1 nm (P/N: 3030A). All poly[(methyl methacrylate)-*co*-(butyl acrylate)-*co*-(methacrylic acid)]-nanoparticles (MMA/BA/MAA statistical copolymer nanoparticles) were obtained from DSM Coating Resins (Waalwijk, The Netherlands).

2.3. Procedures

2.3.1. Synthesis of the MMA/BA/MAA nanoparticles

Two main sets of samples were prepared, both from a similar monomer composition, *i.e.* a mixture of methyl methacrylate (around 67% by weight), n-butyl acrylate (around 30 wt%) and methacrylic acid (around 3 wt%). In both sets the monomers were gradually fed as a pre-emulsified monomer feed to a pre-formed seed.

Sample set 1 had a variation in the amount of chain-transfer agent (1-dodecanethiol, DT) from 0.25 to 1 wt% on total monomer concentration to regulate the molecular weight, as well as a variation in amount of surfactant (sodium dodecyl sulfate, SDS) from 0.35 to 0.41 wt% to tune or control the particle size.

Sample set 2 was more focused on variation in particle size, while maintaining similar levels of DT at 0.50 wt% relative to the total amount of monomers. The variation in particle size was obtained by using different concentrations of pre-formed seed charge. This pre-formed seed was synthesized from a similar monomer composition (MMA/BA/MAA) with DT (0.5 wt%) and ammonium persulfate (0.45 wt%), and using sodium dodecyl sulfate (3 wt%) as surfactant to control the particle size. pH of the prepared seed was adjusted to 8.5 with ammonia. Final particle size of the pre-formed seed was determined to be 27 nm with dynamic light scattering (DLS). Depending on the required particle size, the amount of pre-formed seed in the synthesis of the acrylic emulsion was 0.08%, 0.6% or 10% (all % are wt% solid seed with respect to the total concentration of monomer in the acrylic emulsion), resulting in a final average particle size, as measured via DLS, of 313 nm, 158 nm, and 83 nm, respectively. For all acrylic emulsions in sample set 2 the concentration of DT, surfactant and ammonium persulfate applied during the synthesis was kept constant at 0.5%, 0.1% and 0.3%, respectively (solids relative to total monomers).

2.3.2. Preparation methods

For creating a calibration curve, all PS standards were dissolved in THF at concentrations of approximately 0.2 mg·mL^{-1}. A stock solution of HDC buffer was created by dissolving 6.2 g of sodium dihydrogen orthophosphate, 10.0 g sodium dodecyl sulfate, 134 mL Brij 35 non-ionic surfactant solution and 4.0 g sodium azide in 866.7 mL MilliQ purified water. The stock solution was diluted 20 times with MilliQ purified water before use. Both the polystyrene-nanoparticle standards and the MMA/BA/MAA-nanoparticle samples were diluted 10 times in water prior to injection.

2.3.3. Chromatographic methods

The pump designations used in this section refer to Fig. 1. For the HDC×SEC experiments, the ^{1}D pump (pump A) operated at a flow rate of 40 µL min^{-1}, with a preceding flush program for the first 11.75 min at 1.0 mL min^{-1}. This is reflected in the flow-rate program shown in Table 2. The second-dimension flow rate (supplied by Pump D) was 850 µL min^{-1}. The modulation time was 90 s. The injection volume was 10 µL. The mobile phase for pump A was a surfactant buffer as described in section 2.3.2. The mobile phase for pumps B and D was unstabilized THF; for pump D 0.1% (by volume) of TFA was added to the THF. Pump C delivered a 10-mM formate buffer, brought to pH = 3 with formic acid. For the final sample measurements a modulation time of 0.5 min was used.

It is important to note that neither the ^{2}D column volume, nor the flow rate were adjusted. Instead, the principle of overlapping injections was applied. This concept is described in our previous

Table 1
Overview of MMA/BA/MAA nanoparticle samples.

Sample	Set	DT (wt%)	SDS (wt%)	Concentration of pre-formed seed (wt%)
1	1	0.25	0.41	0 (seed was in-situ prepared)
2	1	0.50	0.41	0 (seed was in-situ prepared)
3	1	0.75	0.41	0 (seed was in-situ prepared)
4	1	1.0	0.38	0 (seed was in-situ prepared)
5	1	0.75	0.35	0 (seed was in-situ prepared)
6	2	0.50	0.1	10
7	2	0.50	0.1	0.6
8	2	0.50	0.1	0.08

Table 2
Flow-rate program used for the analytical method to avoid counter-flow migration of THF into the first-dimension column. For pump designation see Fig. 1.

t (min)	^{A}F (μL·min^{-1})	^{B}F (μL·min^{-1})	^{C}F (μL·min^{-1})
0.00	1000	0	0
11.75	1000	0	0
11.80	*Valve 1 switches from bypass to the main system*		
11.90	40	0	0
12.00	40	80	0
12.10	40	160	800
12.25	40	160	1800

work [8]. Briefly, it is based on the fact that SEC separations typically do not use the separation space in the range $0 < \tau < 0.5$, where τ is the ratio between analyte elution time, t_e (or volume, V_e), and the column dead time or hold-up time, t_0 (or volume, V_0), *i.e.* $\tau = t_e/t_0 = V_e/V_0$ and $\tau = 1$ corresponds to t_0. Assuming that no peaks will elute in this range, a new modulation can be started before the previous one is finished. Consequently, the second-dimension column can contain the contents of up to three modulations simultaneously. As the MMA/BA/MAA-nanoparticle samples were not containing significant amounts of polymers in the range below $\log M = 4$, we extended the unused domain to $0 < \tau < 0.6$, slightly reducing the molecular-weight range covered. This explains why, for a modulation time of 0.5 min, in the results shown further on, the molecular-weight ranges do not extend below $\log M = 4$. From the discussion above it can also be noted that in a worst-case scenario, where a polymer distribution is broader and more separation space is required, the benefit of overlapping injections is less. However, in genuine SEC (with adsorption effects absent) at least half the time can typically be saved.

Calibration curves were recorded under separation conditions that were representative for those used in the actual HDC×SEC system. Thus, for the HDC separation, all nanoparticle standards were analysed using the above-described system, but with a DAD coupled directly to the waste-port of the first valve, which was not switching during these experiments. To calibrate the SEC separation, the autosampler was directly coupled to Mixer 2, which combined the main stream of effluent with the flow from pump C. Pump B was used to deliver solvent to the autosampler. Second-dimension modulations were programmed to start directly after injection. As a result, the calibration setup mimicked almost precisely the actual HDC×SEC system, incorporating the effects of mixing with acidic buffer, subsequent trapping and transfer to the SEC column using an almost identical sample matrix.

2.4. Data treatment

Data obtained from LC×LC experiments were processed and analysed by the 2D-LC data-analysis module of the PIOTR software [14] written in-house in a MATLAB 2017a environment (Mathworks, Woodshole, MA, USA). See section 3.2 for a more extensive explanation of the data-processing steps.

3. Results & discussion

3.1. Development of the system

3.1.1. Processing of HDC effluent: flow and pressure restrictions

Hydrodynamic chromatography (HDC) utilizes a narrow separation domain, roughly between $0.8 < \tau < 1.0$. In the present case, the HDC selectivity window did not extend below $\tau = 0.87$. The HDC column had a dead volume of approximately 13.8 mL and thus the first 11.9 mL was flushed through, as this part of the effluent does not contain analyte.

After HDC separation by particle size, destabilization of the nanoparticle dispersion to yield a solution of constituting polymers is accomplished through the addition of THF in a ratio of approximately 1:9 [aqueous buffer/THF, v/v]. As will be explained later, the resulting flow stream was subsequently mixed in-line with a large flow of acidic formate buffer (pH = 3.0). These two high-volume mixing flows are situated downstream from the first-dimension column and they were found to generate a significant pressure drop.

Consequently, it is feasible for small amounts of THF to migrate against the flow direction from the T-piece that connects the HDC effluent with the THF make-up flow, especially upon switching the first 8-port valve (Valve 1) from waste to analysis position. Over time, this led to a significantly decreased performance of the polymeric-based HDC column, due to dissolution/swelling of the packing material in THF. To counter this, a step-wise flow program (Table 1) was devised and a restriction capillary was installed between the HDC column and the remainder of the system.

3.1.2. Active-modulation and mixing

In practice, implementation of LC×LC is often plagued by several factors [15]. Most important for the present application are (*i*) greatly reduced detection sensitivity relative to one-dimensional LC due to additional dilution and (*ii*) incompatibility of the first-dimension effluent and the second-dimension phase system.

Both problems can be solved by replacing the generic storage loops, which simply ("passively") split the ^{1}D effluent in fractions, with stationary-phase-containing cartridges, referred to as traps. The volume of these traps including the tubing is in the order of several microliters, as opposed to the 40–80 μL of typical storage loops. The latter must be large enough to store the entirety of the ^{1}D effluent. Active stationary-phase-assisted modulation ("SPAM", [16]) is advantageous, because (*i*) the incompatibility of the phase systems can be alleviated, (*ii*) the effective analyte concentration is significantly increased, thus enhancing detection sensitivity, and (*iii*) the volume of the storage loops is no longer a limiting factor in developing first- and second-dimension separation methods.

Active-solvent modulation (ASM, [17]) has also emerged as a useful active-modulation technique to tackle some of the issues above. However, ASM requires a weak ^{2}D eluent for analyte focusing and this is not compatible with SEC [18]. Moreover, to avoid adsorption effects large amounts of THF would be required to reduce the aqueous fraction to similar levels as obtained with SPAM, where the ^{1}D effluent is almost entirely removed. Our studies thus focused on the use of SPAM.

These advantages are countered by several disadvantages. First of all, the traps are prone to clogging and they are found to reduce the overall robustness of the system. Secondly, the traps should be as identical as possible to avoid asymmetry effects in the modulation. The most important limitation, however, is that all analytes that may be present in the first-dimension effluent must be sufficiently retained by the stationary phase used in the trap cartridges.

The latter can be influenced by admixing solvents that enhance retention. With the polymers comprising butyl acrylate (BA), methacrylic acid (MAA) and methyl methacrylate (MMA) monomer units, the overall composition contained both hydrophobic, hydrophilic and charged parts at pH = 7 in the ^{1}D effluent. To facilitate sufficient retention on the traps we opted to use an acidic formate buffer (pH = 3) at a ratio of [HDC-eluent/THF]/formate-buffer 1:10 [v/v] to protonate the acid groups. To monitor for premature elution from the traps an ELS detector was coupled to the waste-port of Valve 2.

It should be noted that during each modulation, 40 μL per minute of effluent volume is first diluted (in two stages) by a factor

of 50, in order to then concentrate all analytes in a volume down to a few μL on an extremely small trapping cartridge, whilst simultaneously destabilizing the nanoparticles and almost entirely removing the incompatible aqueous mobile phase from the plug.

The modulation time proved to be a critical parameter, influencing both the chromatographic performance and the data analysis. Fig. 2 displays the HDC×SEC separation of one of the MMA/BA/MAA-nanoparticle samples using modulation times of 1.5 (A), 1.0 (B), and 0.5 min (C). Longer modulation times require the traps to retain greater amounts of analytes from the ^{1}D effluent. The physical state of the adsorbed matter can be affected by the local concentration, especially in case of polymers. Also, the robustness of the system is reduced at longer modulation times. This becomes apparent from the backpressure trace obtained for the experiment conducted using a modulation time of 1.5 min, shown in Fig. 3.

The backpressure was found to rise dramatically as the trap, positioned in-line after the first-dimension separation, was filled with eluting polymers (Fig. 3B). Subsequent modulations were found to vary significantly in performance, which in turn is reflected in the separations shown in Fig. 2A and B Fig. 2D shows the reconstructed first-dimension chromatograms, where each data point represents the sum of the intensities of a modulation. The experiment with a 1.5 min modulation time (Fig. 2D, ◊) gave rise to a misleading split in the apparent distribution as a result of the inadequate performance of the traps. Such effects are not observed with a modulation time of 0.5 min (Fig. 2D, ■).

3.2. Automated data processing

Distributions observed in raw HDC chromatograms are typically much broader than expected as a result of band-broadening and

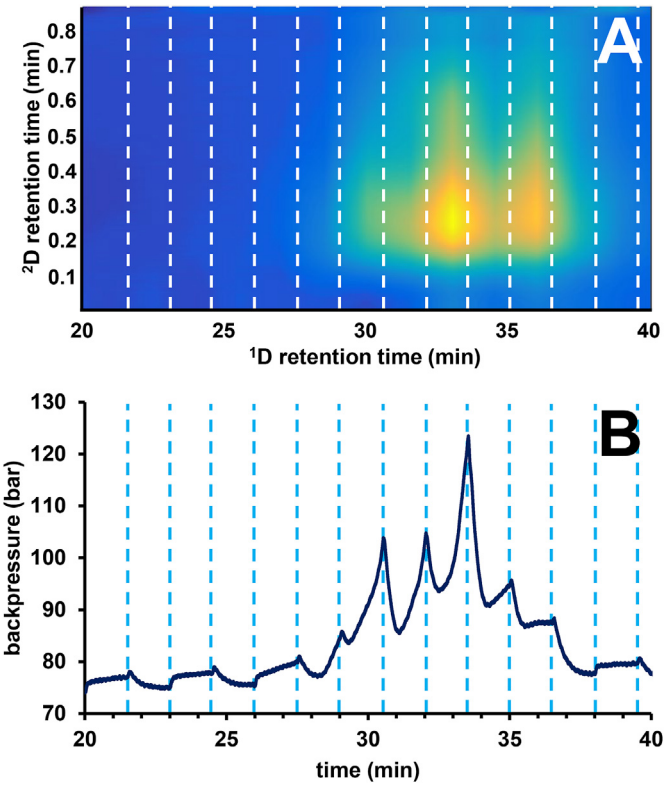

Fig. 3. (A) Section of a HDC×SEC chromatogram of a MMA/BA/MAA-nanoparticle sample, with (B) the corresponding trace of backpressure as a function of time. The dashed, vertical lines indicate the modulations taken at a modulation time of 1.5 min.

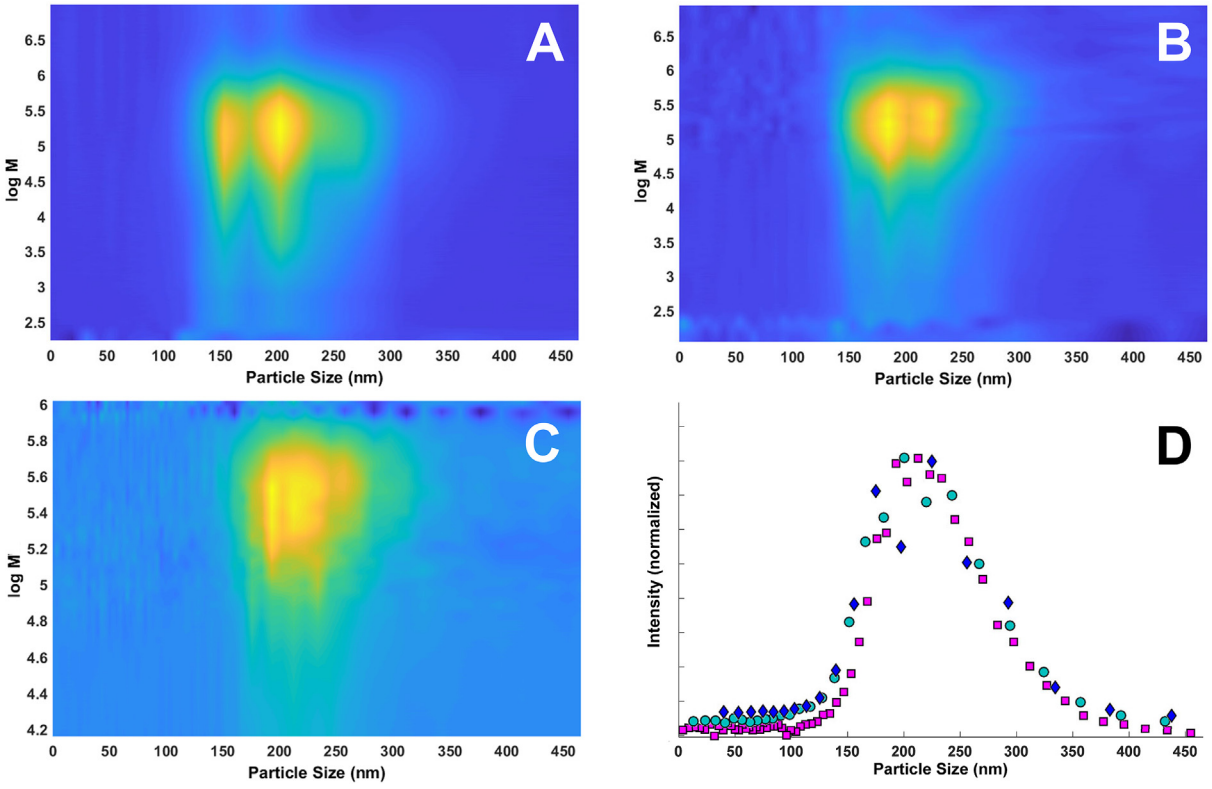

Fig. 2. Effect of modulation time on trap performance and representation of the particle-size distribution (PSD). HDC×SEC separation of a BA/MMA/MAA-nanoparticle test sample using modulation times of A) 1.5, B) 1.0 and C) 0.5 min. D) Reconstructed first-dimension HDC chromatogram with each point representing the sum of intensities per modulation with a modulation time of 1.5 min (◊), 1.0 min (●) and 0.5 min (■). Undersampling and chromatographic-distortion effects can be observed as the modulation time is increased.

non-ideal detector response. For example, in our previous work [8], HDC×SEC analysis of certified NanoSphere nanoparticle standards yielded PSDs with widths up to 200 nm, whereas the standards have a particle size that is certified within a range of 10 nm. Such band broadening can be corrected in 1D-HDC [13], but in case of 2D-LC great care is needed to correctly take into account the second-dimension separation.

We developed an algorithm to automatically process all slices of the 2D-LC separation. The procedure is schematically depicted in Fig. 4A and illustrated for one sample in Fig. 4B–E. In the raw data set (Fig. 4B), the algorithm uses the ranges of validity of the calibration curves from both the ^{1}D-HDC separation and the ^{2}D-SEC separation to automatically extract the separation space covered by the calibration curves (Fig. 4B, highlighted box, resulting in Fig. 4C). Next, the calibration curves are applied to translate the *x*- and *y*-axes (Fig. 4D) to polymer size and molecular weight, respectively.

The selected and calibrated data consists of a matrix of *m* columns representing the modulations and *n* rows depicting the slices. The number *n* is proportional to the number of data points acquired by the detector per modulation (Equation (1)). Each slice is processed and corrected for band-broadening and detector-response effects, as described by McGowan and Langhorst [13]. In short, a calibration curve is constructed by measuring the PSD of particle standards with certified PSDs. The ratio of the measured width of the PSD to the certified width is used to define a band-broadening factor (BBF) as a function of particle size. For any given chromatographic peak, a suitable mathematical distribution function is fitted to the chromatographic peak. The bandwidth parameter of this distribution is then corrected using the BBF and optionally also corrected by a detection-response factor.

However, with approximately 3000–9000 slices to process (depending on the modulation time, which ranges from 0.5 to

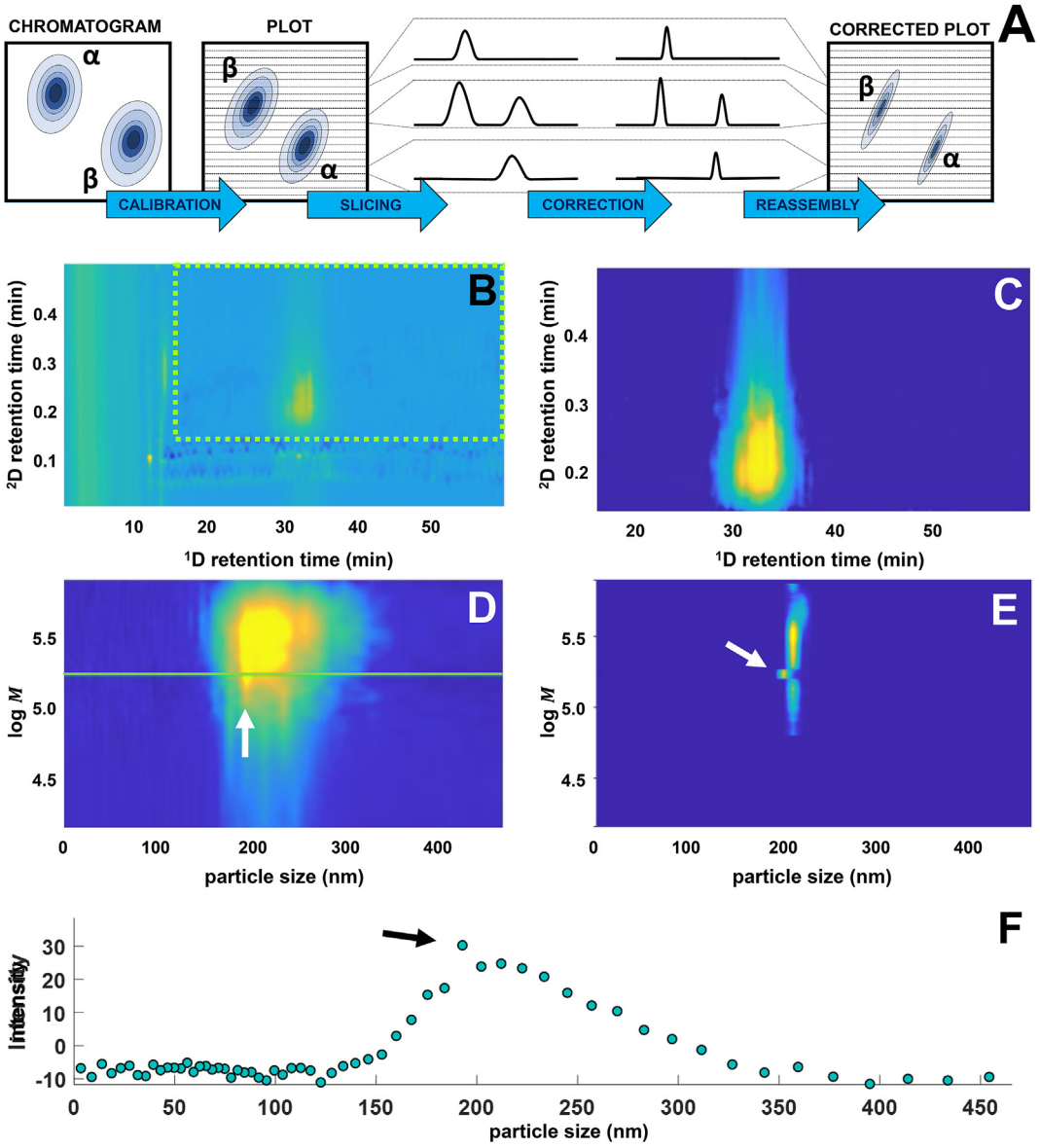

Fig. 4. A) Schematic representation of data-processing procedure. B) Example of raw data, C) Automatically extracted section from raw data based on the time domains covered by the calibration curves of both dimensions, D) application of calibration curves on data, E) example of corrected data, F) ^{1}D slice of plot shown in Fig. 4D (green line) containing an erroneous point which derails the automated curve-fitting algorithm responsible for the visible deviation in Fig. 4E (see arrow). (For interpretation of the references to colour in this figure legend, the reader is referred to the Web version of this article.)

1.5 min), the algorithm must automatically recognize the presence and shape of chromatographic distributions, so as to allow suitable mathematical distributions to be fitted.

To accomplish this, the algorithm was programmed to detect downward zero-crossings in a sliding-average-smoothed first derivative of the data vector (*i.e.* slice n_i). Once a peak is found, a least-squares curve-fitting strategy is applied around the apex of the peak. The algorithm attempts to fit several types of distributions, including several forms of Gaussian and Lorentzian functions and a modified Pearson type-VII distribution. The latter function was adapted from McGowan and Langhorst [13] to yield Equation (2).

$$y = h\left(1 + \frac{(x-\mu)^2}{M(\sigma + E(x-\mu))^2}\right)^{-M} \quad (2)$$

Here, h represents the height of the peak, E the particle size (identical to the location of the apex of the peak), E the shape factor and M the asymmetry factor. The algorithm can accommodate variations in E and M, but typical values were 0.15 and 5, respectively. Generally, the algorithm found Equation (2) to describe the chromatographic peaks successfully. By correlating x to the BBF, the σ-value was corrected and stored for slice n, along with all other parameters and the function-type. The matrix to construct Fig. 4E thus only contained the peak parameters for all slices.

The algorithm generally worked well, but it did prove vulnerable to imperfections in the data, as illustrated in Fig. 4D–F. In Fig. 4D, one of the modulations (see arrow) appears to perform anomalously. This can also be seen from the relevant slice (Fig. 4D, green line) shown in Fig. 4F (anomaly again depicted by arrow). As a result, the curve-fitting protocol is compromised, which results in the plot shown in Fig. 4E. Such erroneous slices are most likely due to modulation issues, as discussed in the previous section. Further study is required to address this weak point of the overall system. Moreover, it should be noted that the algorithm is not capable to recognize the source of, for example, tailing in a recognized distribution. Any such chromatographic tailing would also be present in the band-broadening factor calibration curve and thus should automatically be corrected for. Nevertheless, the algorithm does not make a distinction between chromatographic tailing or tailing as a result of a particular statistical distribution followed by the polymerization or particle growth kinetics. Further studies are required to equip the algorithm with the ability to recognize this.

3.3. Application

The application of this analytical set-up was studied for two series of acrylate copolymer emulsions, where the particle size was varied through adjusting the level of surfactant or seed charge, and/or where the molecular weight was varied by the amount of chain transfer agent (DT) applied. Within both series, the concentration of initiator was kept constant to ensure a comparable radical flux and the final solids level was kept constant. To verify whether the first-dimension HDC separation was correctly carried out, and correctly sampled by second-dimension SEC measurements, and whether calibration on this data was acceptable, all measured particle sizes were compared to those found from 1D-HDC analysis. The results are shown in Fig. 5. A good correlation is observed between the two analytical techniques.

The results from the HDC×SEC experiments are shown in Fig. 6 for sample set 1 (A) and set 2 (B). The measured particle size (PS) and the molecular weight follow the expected trends. Namely, at comparable PS the average weight-average molecular weight (M_w) of the final emulsion polymer in sample set 1, increases with decreasing concentration of chain-transfer agent (samples 1, 2, 3 and 4, see Table 1), and similarly at a constant concentration of CTA (0.75%) the PS increases with decreasing concentration of surfactant (3 and 5).

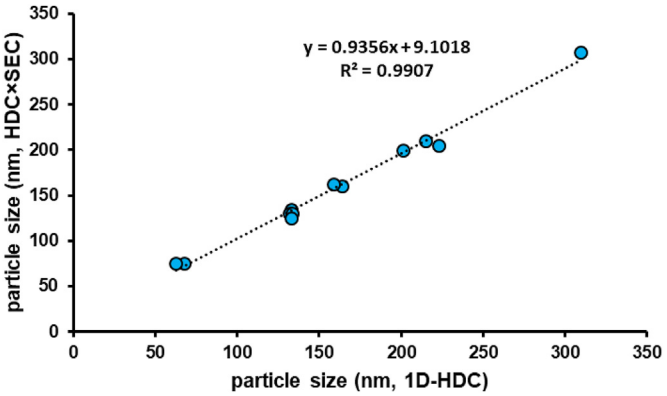

Fig. 5. Particle sizes for all BA/MMA/MAA particles as measured by one-dimensional HDC and two-dimensional HDC×SEC. The strong correlation confirms the integrity of the HDC separation and adequate sampling of the ^{1}D effluent in the HDC×SEC method. Data displays average of two repetitions from HDC×SEC.

The analysis data also reveal a consistent trend for all samples, namely that within a single population of particles, M_w increases with particle size. This trend is clearly seen in the analysis results for series 2 samples 6, 7 and 8 where M_W increases with increasing particle size, not only between the samples but especially within a single sample. The increase in M_n is even more pronounced than that in M_w, resulting in a decrease in PDI (more narrow MWD) with increased particle size.

When attempting to explain these results, one has to consider the rather complex kinetic and mechanistic aspects of the emulsion-polymerization process. In this process, the resulting degree of polymerization (and thus the molecular weight) is strongly dependent on the monomer concentration in the particles and the rate of radical entry into the monomer-swollen particles. According to the widely applied Smith-Ewart case-2 kinetics [19], the average number of free radicals per monomer-swollen particle is one-half, meaning that growth in the particles follows an on-off mechanism, where growth of a polymer chain continues until a second radical is captured inside the particle and stops the chain growth via instantaneous termination. The average number of radicals per particle will, however, increase with increasing particle size, especially when particles become much larger, in which case termination of chain growth may not be instantaneous. Although in the literature there is so far no clear agreement on the overall kinetics and mechanism of emulsion polymerization of methacrylate monomers, such as methyl methacrylate [20], the results reported in this paper are at least partially in line with those reported by Loebach [21]. The latter author investigated the relation between particle size and molecular weight for emulsion polymerization of styrene and found experimentally that, for a finished batch process, the highest molecular weight is found in the largest particles. A possible explanation for this trend, that is consistently seen for the samples analysed in the present study, is that particles that are larger than average may have grown longer and faster due to a higher average number of radicals per time interval.

4. Conclusion

For accurately tailoring the nanoparticle dispersion to the target specification, a profound understanding of nanoparticle formation is indispensable. A method is presented to determine the complete relation between the size distribution of polymeric nanoparticles

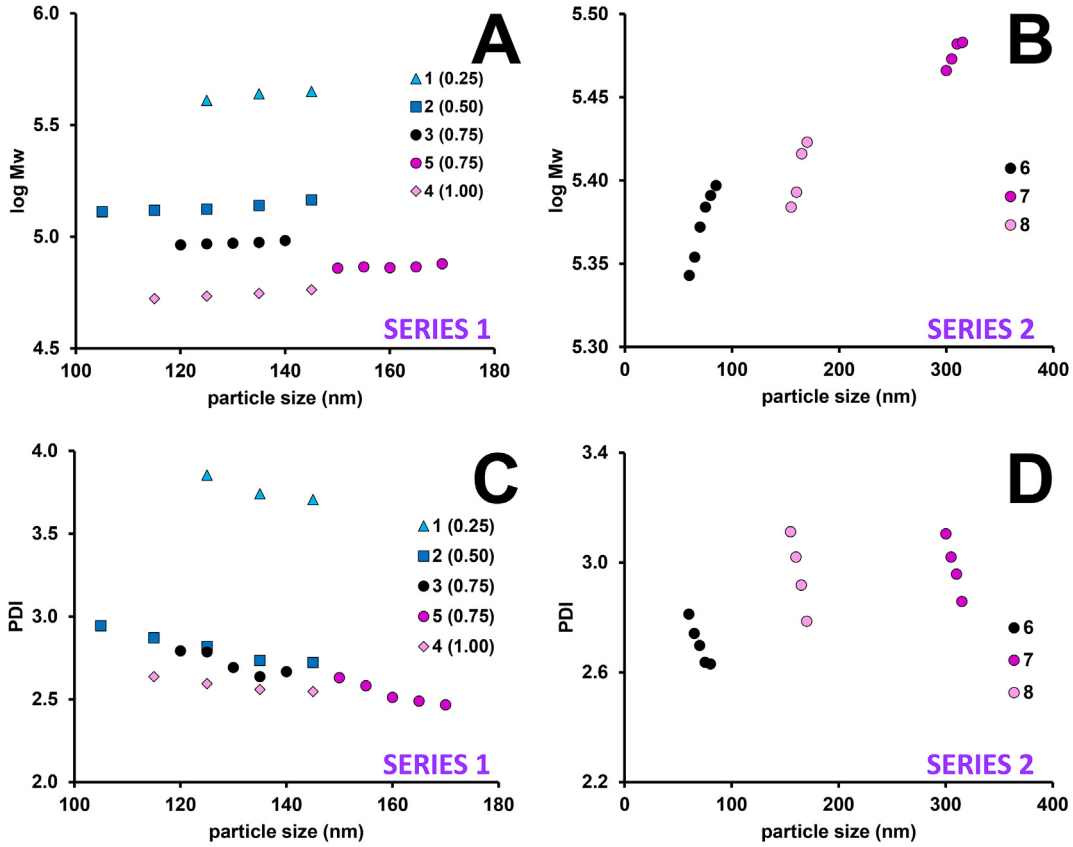

Fig. 6. Results from HDC×SEC analysis for sample set 1 (Panels A and C) and 2 (Panels B and D). Particle size plotted against logM_w (Panels A and B) and particle size plotted against the polydispersity (PDI) (Panels C and D).

and the molecular-weight distribution of the constituting molecules. The method is suitable for particle formulations that contain any kinds of units, be they hydrophobic, hydrophilic or charged. To enhance the accuracy of the measured distributions an algorithm was developed that divides calibrated two-dimensional data in a series of virtual first-dimension chromatograms and allows band-broadening reduction to be carried out. The corrected data is reassembled and the comprehensive two-dimensional relation between nanoparticle size and polymer molecular-weight is obtained. The method was demonstrated using stabilized dispersions of industrial poly[(methyl methacrylate)-*co*-(butyl acrylate)-*co*-(methacrylic acid)]-nanoparticles in water.

It is demonstrated that the proposed approach enables fundamental studies into the process of particle formation and polymer growth during emulsion polymerization. New insights can be obtained in nanoparticle formulations with very narrow particle-size distributions, which are particularly difficult to study by other means.

Declaration of interests

The authors declare that they have no known competing financial interests or personal relationships that could have appeared to influence the work reported in this paper.

Acknowledgement

The MANIAC project is funded by the Netherlands Organisation for Scientific Research in the framework of the Programmatic Technology Area PTA-COAST3 of the Fund New Chemical Innovations (Project 053.21.113). Noor Abdulhussain acknowledges the STAMP project, which is funded under the Horizon 2020 – Excellent-Science program of the European Research Council (ERC), Project 694151. The sole responsibility of this publication lies with the authors. The European Union is not responsible for any use that may be made of the information contained therein. DSM Coating Resins, Waalwijk, is kindly acknowledged for providing the nanoparticle samples. Erik Graafmans is acknowledged for his help with the sample selection and interpretation of the data. Denice van Herwerden and Chris Lukken are acknowledged for their assistance during various stages of the project.

References

[1] N. Elvassore, A. Bertucco, P. Caliceti, Production of insulin-loaded poly(-ethylene glycol)/poly (l-lactide) (PEG/PLA) nanoparticles by gas antisolvent techniques, J. Pharm. Sci. 90 (2001) 1628–1636.
[2] D.A. Edwards, Large porous particles for pulmonary drug delivery, Science 276 (80) (1997) 1868–1872, https://doi.org/10.1126/science.276.5320.1868.
[3] A.J. Defusco, K.C. Sehgal, D.R. Bassett, Overview of uses of polymer latexes, in: J.M. Asua (Ed.), Polym. Dispersions Princ. Appl., Springer Netherlands, Dordrecht, 1997, pp. 379–419, https://doi.org/10.1007/978-94-011-5512-0.
[4] A. Coll, S. Bermejo, D. Hernández, L. Castañer, Colloidal crystals by electrospraying polystyrene nanofluids, Nanoscale Res. Lett. 8 (2013) 26, https://doi.org/10.1186/1556-276X-8-26.
[5] J.P. Rao, K.E. Geckeler, Polymer nanoparticles: preparation techniques and size-control parameters, Prog. Polym. Sci. 36 (2011) 887–913, https://doi.org/10.1016/j.progpolymsci.2011.01.001.
[6] H. Small, Hydrodynamic chromatography a technique for size analysis of colloidal particles, J. Colloid Interface Sci. 48 (1974) 147–161, https://doi.org/10.1016/0021-9797(74)90337-3.
[7] J.C. Giddings, Sample dimensionality: a predictor of order-disorder in component peak distribution in multidimensional separation, J. Chromatogr., A 703 (1995) 3–15, https://doi.org/10.1016/0021-9673(95)00249-M.
[8] B.W.J. Pirok, N. Abdulhussain, T. Aalbers, B. Wouters, R.A.H. Peters,

P.J. Schoenmakers, Nanoparticle analysis by online comprehensive two-dimensional liquid chromatography combining hydrodynamic chromatography and size-exclusion chromatography with intermediate sample transformation, Anal. Chem. 89 (2017) 9167–9174, https://doi.org/10.1021/acs.analchem.7b01906.

[9] D.R. Stoll, P.W. Carr, Two-dimensional liquid chromatography: a state of the art tutorial, Anal. Chem. 89 (2017) 519–531, https://doi.org/10.1021/acs.analchem.6b03506.

[10] R.E. Murphy, M.R. Schure, J.P. Foley, Effect of sampling rate on resolution in comprehensive two-dimensional liquid chromatography, Anal. Chem. 70 (1998) 1585–1594, https://doi.org/10.1021/ac971184b.

[11] G. Vivó-Truyols, S. van der Wal, P.J. Schoenmakers, Comprehensive study on the optimization of online two-dimensional liquid chromatographic systems considering losses in theoretical peak capacity in first- and second-dimensions: a pareto-optimality approach, Anal. Chem. 82 (2010) 8525–8536, https://doi.org/10.1021/ac101420f.

[12] B.W.J. Pirok, A.F.G. Gargano, P.J. Schoenmakers, Optimizing separations in online comprehensive two-dimensional liquid chromatography, J. Separ. Sci. 41 (2018) 68–98, https://doi.org/10.1002/jssc.201700863.

[13] G.R. McGowan, M.A. Langhorst, Development and application of an integrated, high-speed, computerized hydrodynamic chromatograph, J. Colloid Interface Sci. 89 (1982) 94–106, https://doi.org/10.1016/0021-9797(82)90124-2.

[14] B.W.J. Pirok, S. Pous-Torres, C. Ortiz-Bolsico, G. Vivó-Truyols, P.J. Schoenmakers, Program for the interpretive optimization of two-dimensional resolution, J. Chromatogr., A 1450 (2016) 29–37, https://doi.org/10.1016/j.chroma.2016.04.061.

[15] B.W.J. Pirok, P.J. Schoenmakers, Breaking through the barriers, LC-GC, Eur 31 (2018) 242–249.

[16] R.J. Vonk, A.F.G. Gargano, E. Davydova, H.L. Dekker, S. Eeltink, L.J. de Koning, et al., Comprehensive two-dimensional liquid chromatography with stationary-phase-assisted modulation coupled to high-resolution mass spectrometry applied to proteome analysis of Saccharomyces cerevisiae, Anal. Chem. 87 (2015) 5387–5394, https://doi.org/10.1021/acs.analchem.5b00708.

[17] D.R. Stoll, K. Shoykhet, P. Petersson, S. Buckenmaier, Active solvent modulation: a valve-based approach to improve separation compatibility in two-dimensional liquid chromatography, Anal. Chem. 89 (2017) 9260–9267, https://doi.org/10.1021/acs.analchem.7b02046.

[18] B.W.J. Pirok, D.R. Stoll, P.J. Schoenmakers, Recent developments in two-dimensional liquid chromatography: fundamental improvements for practical applications, Anal. Chem. (2018), https://doi.org/10.1021/acs.analchem.8b04841 acs.analchem.8b04841.

[19] W.V. Smith, R.H. Ewart, Kinetics of emulsion polymerization, J. Chem. Phys. 16 (1948) 592–599, https://doi.org/10.1063/1.1746951.

[20] M.J. Ballard, D.H. Napper, R.G. Gilbert, Kinetics of emulsion polymerization of methyl methacrylate, J. Polym. Sci. Polym. Chem. Ed. 22 (1984) 3225–3253, https://doi.org/10.1002/pol.1984.170221141.

[21] D.V. Loebach, The relationship between particle size and molecular weight in emulsion polymerization, Retrosp. Theses. Diss. 5430 (1975).